

Symmetry of electron bands in graphene: (nearly) free electron vs. tight-binding

Eugene Kogan^{1,2,*} and Vyacheslav M. Silkin^{3,4,5,†}

¹*Jack and Pearl Resnick Institute, Department of Physics, Bar-Ilan University, Ramat-Gan 52900, Israel*

²*Max-Planck-Institut für Physik komplexer Systeme, Dresden 01187, Germany*

³*Donostia International Physics Center (DIPC),*

Paseo de Manuel Lardizabal 4, 20018 San Sebastián/Donostia, Spain

⁴*Departamento de Polímeros y Materiales Avanzados: Física,*

Química y Tecnología, Facultad de Ciencias Químicas,

Universidad del País Vasco (UPV/EHU), Apartado 1072,

20080 San Sebastián/Donostia, Basque Country, Spain

⁵*IKERBASQUE, Basque Foundation for Science, 48009 Bilbao, Basque Country, Spain*

(Dated: October 21, 2020)

We present the symmetry labelling of all electron bands in graphene obtained by combining numerical band calculations and analytical analysis based on group theory. The latter was performed both in the framework of the (nearly) free electron model, or in the framework of the tight-binding model. The predictions about relative positions of the bands which can be made on the basis of each of the models just using the group theory (and additional simple qualitative arguments, if necessary) are complimentary.

PACS numbers:

I. INTRODUCTION

The electronic band structure of graphite and a graphite monolayer, called graphene, was a subject of intense study since analytic calculation of Wallace employing a tight-binding model (TBM).¹ In particular, understanding of the symmetries of the electronic energy bands in graphene was of crucial importance. First symmetry classification of them in graphene was presented by Lomer in his seminal paper². Later on the subject was developed in numerous publications.^{3–7} Despite of this, band theory and group-theoretical analysis of two-dimensional hexagonal materials in general, and graphene in particular, continues to attract attention in the very recent years.^{8–21}

In our studies of electronic bands in graphene we combined numerical band calculations with the analytical symmetry analysis of the bands.^{22–24} In Fig. 1 we reproduce the results of the band structure calculations with symmetry labelling following our previous papers,^{23,24} where the details can be found. Here we just remind about the distinction between the σ and the π bands (the former being even with respect to reflection in the plane of graphene, the latter - odd.) Attention is traditionally attracted to the π bands merging at the Fermi level.²⁵ However, we are interested in all the bands (and even in the lowest scattering resonances).

By the analytical symmetry analysis we mean reproduction of the electron band symmetry without solving any differential or even algebraic equations, but just using the group theory (and additional simple qualitative arguments, if necessary). To make such analysis possible, one must chose a model as simple as possible.

There are two alternative approaches to the analysis, both presented, for example, in the book by Kittel.²⁶ One can use either TBM, or the (nearly) free electron

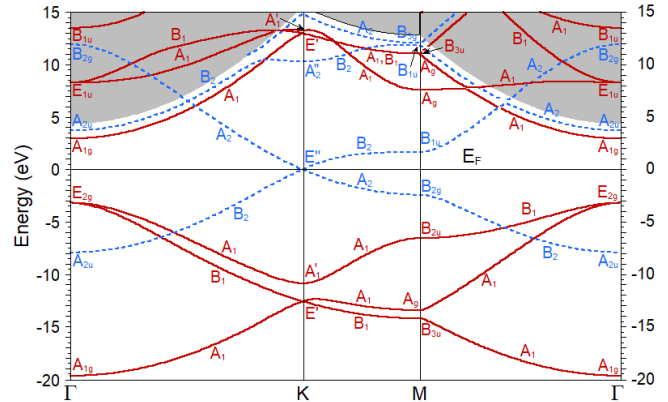


FIG. 1: Calculated graphene band structure with labeling of states at the symmetry points and symmetry directions of the Brillouin zone. The σ -like bands are plotted with red solid lines and the π -like bands - with blue dashed lines. The grey area corresponds to the vacuum continuum states. The black horizontal line shows the Fermi energy position.

model (FEM); note that in spite being just opposite to each other, as a rule, these two approaches give the same result for the bands symmetry.^{26,27}

The minimalistic tight-binding model, with four orbitals on each atoms ($|2s\rangle$, $|2p\rangle$), correctly describes the symmetry of all the occupied bands and the unoccupied π band touching the Fermi level. We call these bands the TBM bands.

However, the minimalistic TBM doesn't describe correctly the other unoccupied bands. The latter are also differ from the TBM bands in their dispersion law and localization with respect to the graphene plane. This is why we called them the FEM bands.^{23,24} To describe the symmetry of all the bands, we used a hybrid approach,

combining TBM and FEM.²⁴ For a very recent review see Ref. 28.

In the present paper we want now to draw attention to the fact, that symmetry analysis of all the bands can be performed alternatively within each of the models - either FEM or TBM (for the latter at the price of extending the basis of atomic orbitals). We compare the predictions (and the predictive power) of the models.

To understand the symmetry classification of the bands, one should remember that the group of wave vector \mathbf{k} at the Γ point is D_{6h} ; at the K point - D_{3h} ; at the point M - D_{2h} . The group of wave vector \mathbf{k} at each of the lines constituting triangle $\Gamma - K - M$ is C_{2v} .^{29,30} Representations of the groups can be found in the book by Landau and Lifshitz.³¹ One of rotations U_2 for the D_{6h} group is about the direction $\Gamma - K$. Rotation C_2^z for the D_{2h} group is about the normal to graphene plane, rotation C_2^x - about the $\Gamma - M$ line. Reflection σ_v for the C_{2v} groups is relative to the plane of graphene.

II. (NEARLY) FREE ELECTRON MODEL

For the sake of the symmetry analysis, we present the wave functions of all the bands in the factorised form

$$\psi_{\mathbf{k}}(x, y, z) = f_{\mathbf{k}}(z)\phi_{\mathbf{k}}(x, y), \quad (1)$$

where $\phi_{\mathbf{k}}(x, y)$ are linear combinations of appropriate plane waves, and the functions $f(z)$ are determined by the boundary conditions $\lim_{z \rightarrow \pm\infty} f_{\mathbf{k}}(z) = 0$. For the σ band $f(z)$ is an even function, and for the π band - an odd one. Analysis of the representations of the groups realised by the plane waves is presented in our previous publications.^{23,24} Notice that the model can equally well incorporate both the TBM bands, localized in graphene, and the FEM bands, having long vacuum tails. The distinction between the two kinds of bands will be reflected in difference between the corresponding functions $f(z)$.

The model potential which would correspond to our choice of the wave functions for the FEM is the sum of two potentials: x, y independent and z -dependent strong potential $V_1(z)$ which localizes the electron states near the graphene plane, and weak potentials $V_2(x, y, z)$ which have graphene lattice symmetry in the x, y plane. Probably, to take into account the existence of carbon ion cores, it would be more correct to consider ψ (and ϕ) as a kind of orthogonalized plane wave, and $V_2(x, y, z)$ as pseudo potentials. If we compare the two lowest σ bands with the two lowest π ones on Fig. 1, the idea to treat the same way both classes of bands looks quite natural.

Extended reciprocal lattice for the honeycomb lattice, we will use, is presented on Fig. 2. Wave functions ϕ of the lowest energy states inside the Brillouin zone (BZ) are just plane waves, at the boundaries of the zone - combinations of two plane waves, and at the band vertexes - of three plane waves.²⁶ Weak lattice potential should lead to small splitting within a doublet or triplet. Fig. 1, with its the lowest singlet at the Γ point, lowest doublet at the

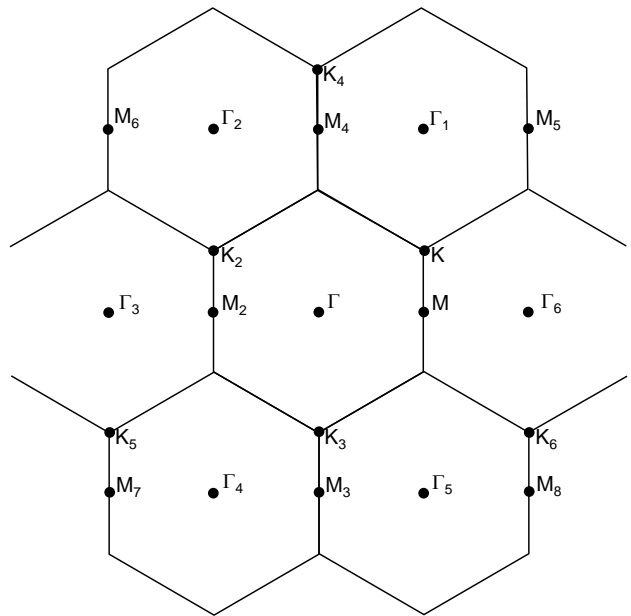


FIG. 2: Extended reciprocal lattice for the honeycomb lattice. The meaning of the symbols see in the text.

$K - M$ line and lowest triplet at the K point, certainly speaks in favor of the applicability of the approach.

More specifically, a single point (or line) in the reduced scheme corresponds to infinite number of points (or lines) in the extended scheme. Thus to a single point Γ in the reduced scheme, in the extended scheme there correspond the $\{\Gamma$ points, $\Gamma_1, \dots, \Gamma_6\}$, etc., to the K point - the points $\{K, K_2, K_3\}$, $\{K_4, K_5, K_6\}$, etc., to the M point - the points $\{M, M_2\}$, $\{M_3, M_4\}$, $\{M_5, M_6\}$, etc. To a single line K_M in the reduced scheme, in the extended scheme there correspond the lines $\{K - M, K_2 - M_1\}$, $\{K_3 - M_3, K_4 - M_4\}$, $\{K_5 - M_7, K_6 - M_8\}$ etc.

At the Γ point, the plane wave $\phi_{\Gamma}(x, y)$ equal identically to 1 realizes representation A_{1g} for even $f(z)$ and representation A_{2u} for odd $f(z)$. At the line $\Gamma - K$ the only basis plane wave $\phi_{\mathbf{k}}(x, y)$ realizes representation A_1 for even $f(z)$ and representation B_1 for odd $f(z)$.

At the K point, $\phi_{\mathbf{K}}(x, y)$ is a linear combination of three plane waves $e^{i\mathbf{K}\cdot\mathbf{r}}$ with the wave vectors corresponding to the three equivalent vertices of the hexagon $\mathbf{K} = \left(\frac{2\pi}{3a}, \frac{2\pi}{3\sqrt{3}a}\right)$, $\mathbf{K}_2 = \left(-\frac{2\pi}{3a}, \frac{2\pi}{3\sqrt{3}a}\right)$, $\mathbf{K}_3 = \left(0, -\frac{4\pi}{3\sqrt{3}a}\right)$. For even $f(z)$ the functions $f(z) \times \{e^{i\mathbf{K}_1\cdot\mathbf{r}}, e^{i\mathbf{K}_2\cdot\mathbf{r}}, e^{i\mathbf{K}_3\cdot\mathbf{r}}\}$ realize $A'_1 + E'$ representations of D_{3h} . For odd $f(z)$ the functions realize $A''_2 + E''$ representations. The π triplet can be substantially higher than the σ triplet corresponding to the same plane waves due to the difference between the energy of odd and even states in the strong $V(z)$ potential.

To find explicitly splitting of the bands at the K point we should solve the secular equation, which, taking into account the symmetry and shifting energy by the diagonal matrix element of the potential, we may write down

in the form

$$\begin{vmatrix} -E & V_2 & V^* \\ V^* & -E & V \\ V & V^* & -E \end{vmatrix} = 0, \quad (2)$$

where V_2 is the matrix element of the potential $V_2(x, y, z)$ between some pair of different states from $\mathbf{K}, \mathbf{K}_2, \mathbf{K}_3$. Using Cardano's formula, we may write down the roots as

$$E = 2\text{Re} \left(\sqrt[3]{V^3} \right), \quad (3)$$

where Re means real part. From the fact that one of the roots should be doubly degenerate, we come to the conclusion that V is real. (Of course, this can be obtained in a more direct way, on the basis of potential's symmetry.) Anyhow, the roots are $E_{1,2} = -V, E_3 = 2V$. We understand that relative positions of the singlet and the doublet depend upon sign of V . If we assume that the matrix element V_2 is positive, we obtain that in each triplet the doublet should be lower than the singlet.

At the M point, $\phi_{\mathbf{K}}(x, y)$ is a linear combination of two plane waves with the wave vectors $\mathbf{M} = (\pm \frac{2\pi}{3a}, 0)$. For even $f(z)$ the function $f(z) \times$ (sum or difference of the exponents) realizes A_g and B_{3u} representations of D_{2h} respectively. For odd $f(z)$ the function $f(z) \times$ (sum or difference of the exponents) realizes B_{1u} and B_{2g} representation of D_{2h} respectively.

The wave functions of the bands at the K point, higher than the lowest triplets, are combinations of the plane waves with the wave vectors $\mathbf{K}_4 = (0, \frac{8\pi}{3\sqrt{3}a})$, $\mathbf{K}_5 = (-\frac{4\pi}{3a}, -\frac{4\pi}{3\sqrt{3}a})$, $\mathbf{K}_6 = (\frac{4\pi}{3a}, -\frac{4\pi}{3\sqrt{3}a})$, which realize representations identical to those realised by the plane waves with the wave vectors $\mathbf{K}, \mathbf{K}_2, \mathbf{K}_3$. This explains the second copy of the representations $A'_1 + E'$ we observe at the K point on Fig. 1.

The wave functions of the bands at the M point, higher than the lowest ones, are combinations of two plane waves with the wave vectors $\mathbf{M}_{3,4} = (0, \pm \frac{2\pi}{\sqrt{3}a})$. For even $f(z)$ the function $f(z) \times$ (sum or difference of the exponents) realizes A_g and B_{2u} representation of D_{2h} respectively. The bands with these symmetries we see on Fig. 1. For odd $f(z)$ the function $f(z) \times$ (sum or difference of the exponents) realizes B_{1u} and B_{3g} representation of D_{2h} respectively.

To describe still higher bands at the M point we consider four additional plane waves $e^{i\mathbf{M} \cdot \mathbf{r}}$, with the wave vectors $\mathbf{M}_{5,\dots,8} = (\pm \frac{4\pi}{3a}, \pm \frac{2\pi}{\sqrt{3}a})$. These four plane waves, multiplied by even function $f(z)$ realize $A_g + B_{1g} + B_{2u} + B_{3u}$ representation of the group D_{2h} .

The wave functions of the bands at the Γ point, higher than the two lowest ones, correspond to combinations of 6 plane waves with the wave vectors $\Gamma_1, \dots, \Gamma_6$, presented on Fig. fig:bandsn, and corresponding to $(\pm \frac{2\pi}{3a}, \pm \frac{2\pi}{\sqrt{3}a})$, $(\pm \frac{4\pi}{3a}, 0)$. For even $f(z)$ the functions (1) realize $A_{1g} +$

$B_{1u} + E_{2g} + E_{1u}$ representations of the group D_{6h} . To find explicitly splitting of the bands at the Γ point we should diagonalize the Hamiltonian, which in the representation $\Gamma_1, \dots, \Gamma_6$ is a circulant 6×6 matrix with the matrix elements

$$\hat{H} = \begin{pmatrix} 0 & V_2^{(a)} & V_2^{(b)} & V_2^{(c)} & V_2^{(b)} & V_2^{(a)} \\ V_2^{(a)} & 0 & V_2^{(a)} & V_2^{(b)} & V_2^{(c)} & V_2^{(b)} \\ V_2^{(b)} & V_2^{(a)} & 0 & V_2^{(a)} & V_2^{(b)} & V_2^{(c)} \\ V_2^{(c)} & V_2^{(b)} & V_2^{(a)} & 0 & V_2^{(a)} & V_2^{(b)} \\ V_2^{(b)} & V_2^{(c)} & V_2^{(b)} & V_2^{(a)} & 0 & V_2^{(a)} \\ V_2^{(a)} & V_2^{(b)} & V_2^{(c)} & V_2^{(b)} & V_2^{(a)} & 0 \end{pmatrix}. \quad (4)$$

Note that due to the symmetry of the problem, there are only 3 different matrix element of $V_2(x, y, z)$: $V_{\Gamma_1-\Gamma_2} \equiv V_2^{(a)}$, $V_{\Gamma_1-\Gamma_3} \equiv V_2^{(b)}$, and $V_{\Gamma_1-\Gamma_4} \equiv V_2^{(c)}$ (we again shifted energy by the diagonal matrix element of the potential). The eigenvalues of the matrix (4) are

$$E_i = V_2^{(a)} r_i + V_2^{(b)} r_i^2 + V_2^{(c)} r_i^3 + V_2^{(b)} r_i^4 + V_2^{(a)} r_i^5, \quad (5)$$

where r_i is one of the distinct solutions of $r^6 = 1$. After simple algebra we obtain

$$\begin{aligned} E_1 &= 2V_2^{(a)} + 2V_2^{(b)} + V_2^{(c)} \\ E_{2,3} &= V_2^{(a)} - V_2^{(b)} - V_2^{(c)} \\ E_{4,5} &= -V_2^{(a)} - V_2^{(b)} + V_2^{(c)} \\ E_6 &= -2V_2^{(a)} + 2V_2^{(b)} - V_2^{(c)}. \end{aligned} \quad (6)$$

Considering only σ bands, we may say that that the eigenfunction corresponding to E_1 realizes A_{1g} representation, the eigenfunctions corresponding to $E_{2,3}$ realize E_{1u} representation, the eigenfunctions corresponding to $E_{3,4}$ realize E_{2g} representation, and the eigenfunction corresponding to E_6 realizes B_{1u} representation of the group D_{6h} .

If we assume that the largest, by absolute value, matrix elements of the potential $V(x, y, z)$ are between the states, with the opposite wave vectors, and negative, we obtain that the three lowest bands are even with respect to rotations by an angle π about the z axis, perpendicular to the graphene plane, and the three others are odd. That is sextuplet is divided into two triplets: the lower one - $A_{1g} + E_{2g}$ and the higher one - $B_{1u} + E_{1u}$.

On the line $K - M$ in the reduced scheme, the lowest doublet would corresponds to two plane waves with the wave vectors on the lines $K - M$ and $K_2 - M_2$. For even $f(z)$, the function $f(z) \times$ (sum of the exponents) realizes A_1 representations, and the function $f(z) \times$ (difference of the exponents) realizes B_1 representation of C_{2v} . For odd $f(z)$, the function $f(z) \times$ (sum of the exponents) realizes B_2 representation, and the function $f(z) \times$ (difference of the exponents) realizes and A_2 representation of the group.

The third band corresponds to the single plane waves with the wave vectors on the lines $K_3 - M_3$, and the fourth

band corresponds to the single plane waves with the wave vectors on the lines $K_4 - M_4$. Both realize representation A_1 .

Then comes doublet corresponding to the plane waves with the wave vectors on the line $K_5 - M_7$ and $K_6 - M_8$. From the point of symmetry it should be identical to the first doublet.

III. TIGHT-BINDING MODEL

In the frame of the tight-binding model we look for the solution of the Schrödinger equation as a linear combination of the functions

$$\psi_{\beta;\mathbf{k}}^j = \sum_{\mathbf{R}_j} e^{i\mathbf{k}\cdot\mathbf{R}_j} \psi_{\beta}(\mathbf{r} - \mathbf{R}_j), \quad (7)$$

where ψ_{β} are atomic orbitals, $j = A, B$ labels the sublattices, and \mathbf{R}_j is the radius vector of an atom in the sublattice j . (Notice that we assume only symmetry of the basis functions with respect to rotations and reflections; the question how these functions are related to the atomic functions of the isolated atom is irrelevant.)

A symmetry transformation of the functions $\psi_{\beta;\mathbf{k}}^j$ is a direct product of two transformations: the transformation of the sub-lattice functions $\phi_{\mathbf{k}}^{A,B}$, where

$$\phi_{\mathbf{k}}^j = \sum_{\mathbf{R}_j} e^{i\mathbf{k}\cdot\mathbf{R}_j}, \quad (8)$$

and the transformation of the orbitals ψ_{β} . Thus the representations realized by the functions (7) will be the direct product of two representations. One should pay attention that the wave vector \mathbf{k} in Eqs. (7) and (8) is reduced to the first BZ, while the wave vector in Eq. (1) was considered as belonging to the infinite plane (extended zone scheme).

We'll start from summing up the results of the symmetry analysis in the framework of the TBM obtained in our previous publications, when the basis included only four atomic orbitals: $|s, p\rangle$.²²⁻²⁴ The σ bands are constructed from the $|2s, 2p_{x,y}\rangle$ orbitals, and the π bands are constructed from the $|p_z\rangle$ orbitals. At the Γ point the representations realised by the σ bands are $A_{1g} + B_{1u}$ (constructed from the $|s\rangle$ orbitals) and $E_{1u} + E_{2g}$ (constructed from the $|p_{x,y}\rangle$ orbitals); the representations realised by the π bands are $A_{2u} + B_{2g}$. At the K point the representations realised by the σ bands are $A'_1 + A'_2$ (constructed from the $|p_{x,y}\rangle$ orbitals) and twice E' (constructed from the $|s, p_{x,y}\rangle$ orbitals); the representation realised by the π bands is E'' . At the M point the representations realised by the σ bands are $A_g + B_{3u}$ (constructed from the $|s\rangle$ orbitals, same representations constructed from the $|p_x\rangle$ orbitals, and $B_{1g} + B_{2u}$ (constructed from the $|p_y\rangle$ orbitals); the representations realised by the π bands are $B_{1u} + B_{2g}$.

Just by counting the number of bands on Fig. 1 we realize that the basis of atomic orbitals should be expanded

to describe additional bands. Actually, the necessity to extend the basis for accurate description of the occupied bands, comparable to the result of calculations based on plane waves is well known (traditionally one chooses two sets of s, p and one set of d) atom-centered basis functions based on the atomic orbitals. However, this choice yields a wrong description of the first unoccupied bands, which start about 3.25 eV above the Fermi level and are parabolic around the BZ center, Γ .³² These bands have long expansion into the vacuum, and are strongly influenced by the image-potential tail³³ with even and odd mirror symmetry in the graphene plane. Moreover, they can be easily influenced by applied electric field,^{34,35} adsorbate deposition,³⁶⁻³⁸ or transformed upon variation of the graphene sheet shape.³⁹ Notice that the first two unoccupied states are important for e.g. the description of interlayer states, reactivity, intercalation,^{40,41} and tunneling into graphene, where the inelastic phonon scattering plays a dominant role.^{42,43} To overcome this defect, there was presented an interesting idea to add long-range orbitals to the minimalistic $|2s, 2p\rangle$ basis.⁴⁴ Notice that the main dynamical effect defining the long tail bands proposed in Ref. 44 is precisely the image potential experienced by an electron due to its image charge in the graphene sheet.^{33,45,46}

Our paper is mostly devoted to FEM, and in the spirit of our emphasis of simple models, we decided, while considering the TBM for comparison, just to add to the minimalistic basis atomic orbitals one by one, to understand which minimal additions are necessary to describe the symmetry of all calculated bands. Analysis of the TBM with the above mentioned long-range orbitals will be the subject of our next publication.

The first choice is obvious - $|3s\rangle$ atomic orbital, to describe redundant σ band, and $|3p_z\rangle$ atomic orbital, to describe redundant π band. As far as the symmetry is concerned, the orbitals give copies of the bands constructed from $|2s\rangle$ and $|2p_z\rangle$ atomic orbitals. The fact, that the symmetry of the two lowest unoccupied bands at the Γ point is identical to the symmetry of the two lowest occupied ones, speaks in favor of such choice.

However, there is a problem with the unoccupied π band at the K point. The $|3p_z\rangle$ atomic orbitals, like $|2p_z\rangle$ orbitals, give doubly degenerate band at the point. To solve the problem we have to introduce $|3d\rangle$ orbitals. In fact, expanding the $D^{(2)}$ representation of the rotations group, the orbitals realise, with respect to irreducible representations of the group D_{3h} ,³¹ we obtain

$$D^{(2)} = A'_1 + E' + E''. \quad (9)$$

We can chose the bases of the representations respectively as

$$|d_{z^2}\rangle; |d_{x^2-y^2}\rangle, |d_{xy}\rangle; |d_{xz}\rangle, |d_{yz}\rangle. \quad (10)$$

The π band should be constructed from the last two orbitals. The functions $\phi_{\mathbf{k}}^{A,B}$ realize E' representation of the group D_{3h} . Thus π bands at the K point realise the

following representations:

$$E' \times E'' = A_1'' + A_2'' + E''. \quad (11)$$

Thus the calculated A_2'' band is accounted for.

IV. COMPARISON BETWEEN THE BAND CALCULATIONS AND THE PREDICTIONS OF THE MODELS

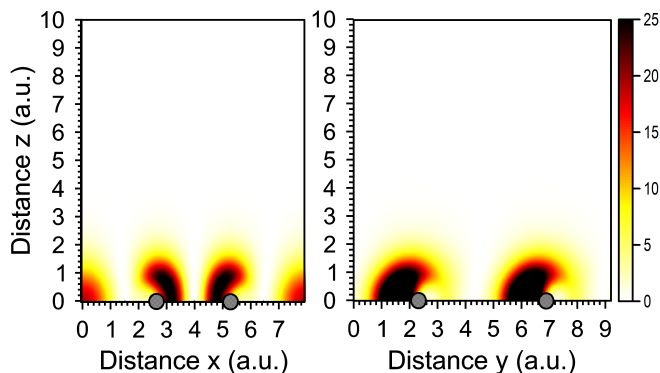


FIG. 3: Charge-density distribution (in arbitrary units) in $x = 0$ plane for the sixth band at the M point. Filled dots show the carbon ion positions.

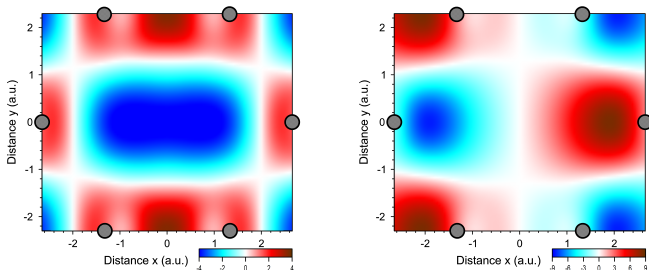


FIG. 4: Real (left) and imaginary (right) parts of the wave function (in arbitrary units) at the $z = 0$ plane for the sixth band at the M point.

The symmetry of each band can be obtained from inspection of the wave function describing the band (at a given value of wave vector) obtained as the result of band calculations. Such analysis was performed in our previous publication for all bands apart from four highest bands at the M point.²⁴ In the present publication we fill this void. On Figs. 3-8 we present the results of the calculations of the density and wave functions of the bands from the sixth to the eighth (counting from below) at the M point. Inspection of the z -dependence of the density shows that these are σ bands. The wave functions of the σ bands are plotted at the plane $z = 0$. For the π bands, the wave function is identically equal to zero at the $z = 0$ plane, so we plotted the wave function at the plane $z = 1$ a.u.

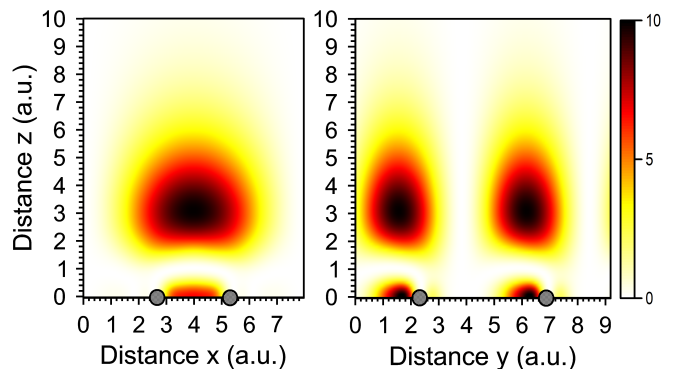


FIG. 5: Charge-density distribution (in arbitrary units) in $x = 0$ plane for the seventh band at the M point. Filled dots show the carbon ion positions.

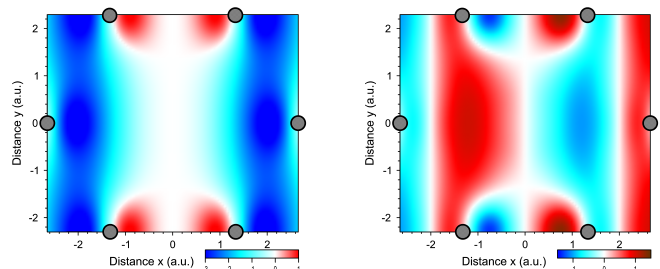


FIG. 6: Real (left) and imaginary (right) parts of the wave function (in arbitrary units) at the $z = 0$ plane for the seventh band at the M point.

For the seventh band the wave function is equal to zero along the y -axis, which corresponds to the representation B_{3u} . (Because the wave function is antisymmetric with respect to reflection, it should be equal to zero at the axis of reflection.) The wave functions of the sixth and eighth band are different from zero everywhere at the plane, which is consistent with the representation A_g .

On Figs. 9 and 11 we present the results of the calculations of the density of the ninth and tenth bands. The wave function is identically equal to zero at the $z = 0$ plane, so it is π band. To find the symmetry of the bands on Figs. 10 and 12 we plot the wave function at the plane $z = 1$ a.u. The wave function of the ninth band is different from zero everywhere at the plane, which is consistent with the representation B_{1u} . For the tenth band the wave function is equal to zero along the y -axis, which corresponds to the representation B_{3g} .

The calculated symmetry of the bands can be explained in the framework of both models. The FEM, in addition, predicts near degeneracy within the groups of the bands (we call such groups multiplets) and positions of such groups relative to each other.

Let us start our analysis from σ bands. At the Γ point the TBM with the $|2s, 2p_{x,y}\rangle$ basis gives $A_{1g} + E_{2g} + B_{1u} + E_{1u}$ bands. The position of the three last bands relative to the three first ones can be understood recall-

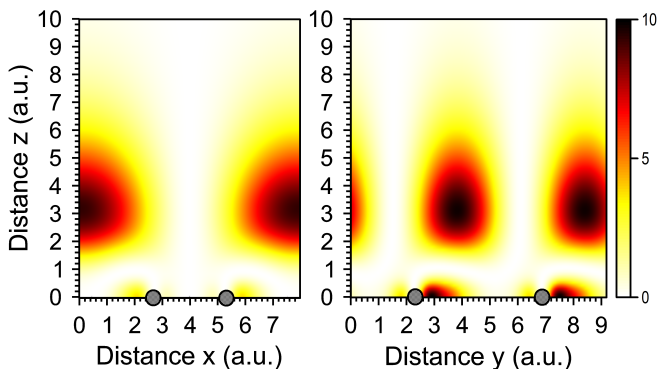


FIG. 7: Charge-density distribution (in arbitrary units) in $x = 0$ plane for the eighth band at the M point. Filled dots show the carbon ion positions.

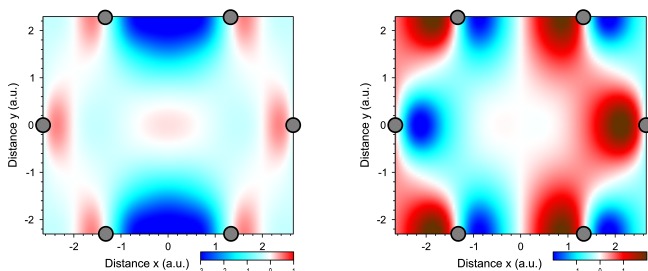


FIG. 8: Real (left) and imaginary (right) parts of the wave function (in arbitrary units) at the $z = 0$ plane for the eighth band at the M point.

ing the distinction between binding and anti-binding orbitals. Addition to the basis of the $|3s\rangle$ orbital gives additionally A_{1g} and B_{1u} bands. We have to assume that the B_{1u} band is swallowed by the continuum.

The FEM gives at the Γ point the lowest band (A_{1g}), then the sextuplet $A_{1g} + E_{2g} + B_{1u} + E_{1u}$. The large energy difference is explained by the fact that the former corresponds to the plane wave with $\mathbf{k} = 0$, and the latter is constructed from plane waves corresponding to the points $\Gamma_1, \dots, \Gamma_6$. The order of the bands in the sextuplet was discussed in Section II. The order within the sextuplet observed on Fig. 1 can be explained in the framework of the FEM by making plausible assumptions about the lattice (pseudo) potential (see Section II).

At the M point the TBM gives three times $A_g + B_{3u}$ bands, constructed from $|2s\rangle$, $|2p_x\rangle$ and $|3p_x\rangle$ orbitals respectively, and $B_{1g} + B_{2u}$ bands, constructed from $|2p_y\rangle$ orbitals. We have to assume that B_{1g} and B_{3u} bands are swallowed by the continuum. The counterintuitive fact is that the band B_{1g} of the $|2p_y\rangle$ origin is swallowed, while one of the bands of the $|3p_x\rangle$ origin isn't.

The FEM gives at the M point the lowest doublet ($A_g + B_{3u}$), then the higher doublet ($A_g + B_{2u}$), and then four still higher bands ($A_g + B_{1g} + B_{2u} + B_{3u}$). We have to assume that the bands B_{1g} and B_{2u} from

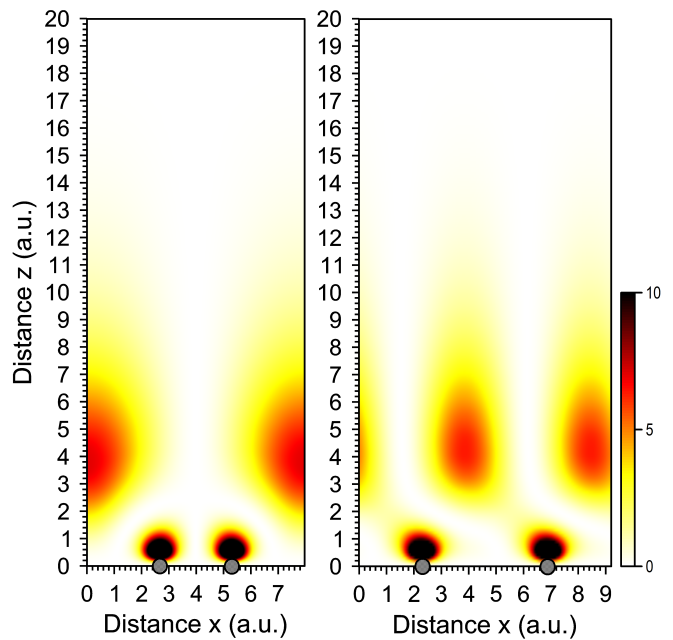


FIG. 9: Charge-density distribution (in arbitrary units) in $x = 0$ plane for the ninth band at the M point. Filled dots show the carbon ion positions.

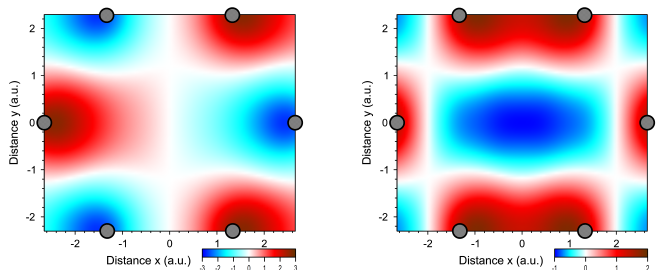


FIG. 10: Real (left) and imaginary (right) parts of the wave function (in arbitrary units) at the $z = 1$ a.u. plane for the ninth band at the M point.

the highest quadruplet are swallowed by the continuum. The distances between the multiplets is explained in the FEM by the fact that the lowest doublet is constructed from the plane waves with the wave vectors corresponding to the points M and M_2 , the second one - M_3 and M_4 , and the quartet - $M_{5, \dots, 8}$. The weak the potential $V(x, y)$ should lead to weak splitting within each multiplet, and also to weak splitting of the lowest doublet along the whole $K - M$ line. The weak splitting of the lowest doublet along the whole $K - M$ line (including the M point), and the weak splitting of the highest doublet at the M point is what we see on Fig. 1. To be honest we must notice that strong splitting of the second doublet at the M point doesn't agree well with the idea of weak (pseudo) potential $V(x, y)$.

At the K point the TBM gives $A'_1 + A_2$ bands of $|2s\rangle$ origin, the bands with the same symmetry of $|3s\rangle$ origin,

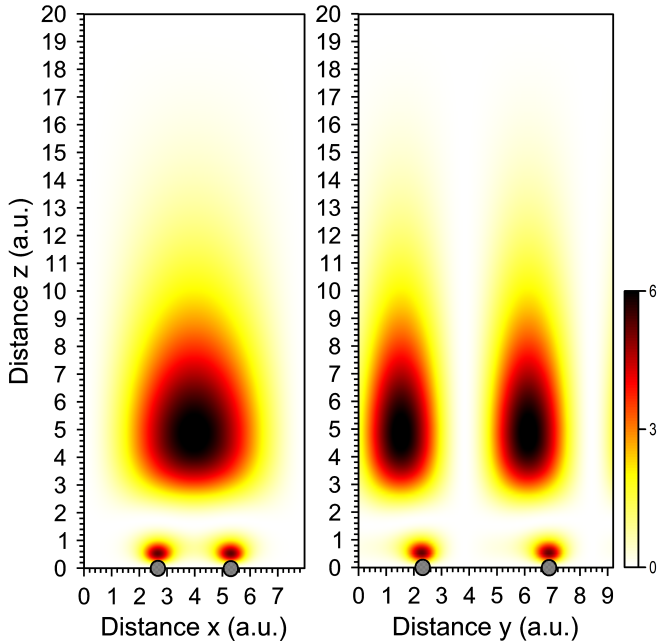


FIG. 11: Charge-density distribution (in arbitrary units) in $x = 0$ plane for the tenth band at the M point. Filled dots show the carbon ion positions.

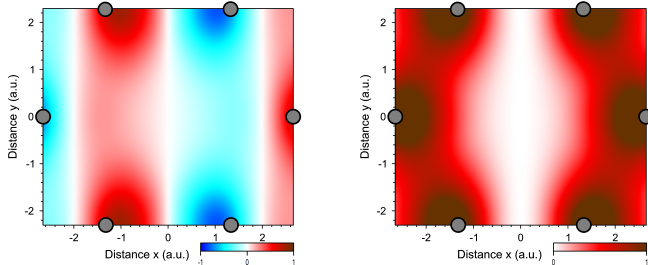


FIG. 12: Real (left) and imaginary (right) parts of the wave function (in arbitrary units) at the $z = 1$ a.u. plane for the tenth band at the M point.

and twice E' bands of of $|p_{x,y}\rangle$ origin. To be in line with the band calculations we have to assume that one of the $|2s\rangle$ bands is swallowed by the continuum, while one of the $|3s\rangle$ bands isn't.

The FEM gives at the K point two triplets with identical symmetry ($A'_1 + E'$). Large distance between the triplets is explained by the fact that the first triplet is constructed from the plane waves corresponding to the points K, K_2, K_3 , and the second triplet is constructed from the plane waves corresponding to the points K_4, K_5, K_6 . The assumption of weak $V(x, y)$ potential leads to prediction that the bands within each triplet will be only weakly split.

The FEM predicts relative the positions of the bands at the line $K - M$: close doublet, higher a single band, still higher the next single band, and then still higher another close doublet. This prediction corresponds to

what we see on Fig. 1.

Now let us come to π bands. At the Γ point the TBM gives $A_{2u} + B_{2g}$ bands constructed from $|2p_z\rangle$ orbitals and bands with the same symmetry constructed from $|3p_z\rangle$ orbitals. We have to assume that B_{2g} $|3p_z\rangle$ bands is swallowed by the continuum. The FEM gives A_{2u} band and sextuplet $A_{2u} + B_{2g} + E_{1u} + E_{2g}$. We have to assume that E_{1u} and E_{2g} bands are swallowed by the continuum.

At the M point the TBM gives $B_{1u} + B_{2g}$ bands, constructed from $|2p_z\rangle$ orbitals, and bands with the same symmetry constructed from $|3p_z\rangle$ orbitals. We have to assume that B_{2g} $|3p_z\rangle$ band is swallowed by the continuum. The FEM gives lower doublet $B_{1u} + B_{2g}$ and the second doublet $B_{1u} + B_{3g}$.

The K point is especially problematic to TBM. More specifically, the two bands merging at the Fermi level and realizing representation E'' are well described as constructed from the $|2p_z\rangle$ orbitals. The problem is with the higher π band. Like it was shown in Section III, to describe the nondegenerate π band at the K point in the framework of the TBM we need $|3d_{xz}\rangle, |3d_{yz}\rangle$ orbitals. But this choice leaves unanswered the question: Why, π band constructed from $|3d\rangle$ orbitals turns out to be lower than that constructed from $|3p_z\rangle$ orbitals? Probably it can be explained by its hybridization with the scattering resonances predicted⁴⁷ and observed⁴⁸⁻⁵⁰ recently in graphene. It would be interesting to clarify this point in the future.

On the other hand, the FEM predicts at the K point the triplet $E'' + A'_2$ which we clearly see on Fig. 1. To be honest we must notice that strong splitting of between the A'_2 and E'' bands doesn't agree well with the idea of weak (pseudo) potential $V(x, y)$.

Looking at the bands at the line $K - M$ on Fig. 1 one sees similarity between π bands and four lowest σ ones. The higher π bands are swallowed by the continuum. Comparing the two alternative approaches to the symmetry classification of the electron bands, we must say that their predictions are complimentary.

V. CONCLUSIONS

We presented the symmetry labelling of all electron bands in graphene obtained by combining numerical band calculations and analytical analysis based on group theory. The emphasize was on the comparison of the predictions of the tight-binding and (nearly) free electron models. The predictions of these two models were found to be complimentary to each others and agreeing well with the results of numerical band calculations.

Acknowledgments

The work on this paper started during E.K. visit to Max-Planck-Institut für Physik komplexer Systeme in

December of 2019 and January of 2020. E.K. cordially thanks the Institute for the hospitality extended to him during that and all his previous visits.

V.M.S. acknowledges support from the Project of the Basque Government for consolidated groups of the Basque University, through the Department of Univer-

sities (Q-NANOFOT IT1164-19) and from the Spanish Ministry of Science and Innovation (Grant No. PID2019-105488GB-I00).

We are grateful to G. J. Ferreira, G. G. Naumis and R.-J. Slager for bringing our attention to their papers.

-
- * Electronic address: Eugene.Kogan@biu.ac.il
 † Electronic address: vyacheslav.silkin@ehu.es
- 1 P. R. Wallace, *Phys. Rev.* **71**, 622 (1947).
 - 2 W. M. Lomer, *Proc. R. Soc. London, Ser. A* **227**, 330 (1955).
 - 3 J. C. Slonczewski and P. R. Weiss, *Phys. Rev.* **109**, 272 (1958).
 - 4 G. Dresselhaus and M. S. Dresselhaus, *Phys. Rev.* **140**, A401 (1965).
 - 5 F. Bassani and G. P. Parravicini, *Nuovo Cimento B* **50**, 95 (1967).
 - 6 L. M. Malard, M. H. D. Guimaraes, D. L. Mafra, M. S. C. Mazzoni, and A. Jorio, *Phys. Rev. B* **79**, 125426 (2009).
 - 7 J. L. Manes, *Phys. Rev. B* **85**, 155118 (2012).
 - 8 D. Goldberg, Y. Bando, Y. Huang, T. Terao, M. Mitome, C. Tang, and C. Zhi, *ACS Nano* **4**, 2979 (2010).
 - 9 P. Vogt, P. De Padova, C. Quaresima, J. Avila, E. Frantzeskakis, M. C. Asensio, A. Resta, B. Ealet, and G. Le Lay, *Phys. Rev. Lett.* **108**, 155501 (2012).
 - 10 S. Chowdhury and D. Jana, *Rep. Prog. Phys.* **79**, 126501 (2016).
 - 11 P. Ayria, S.-i. Tanaka, A. R. T. Nugraha, M. S. Dresselhaus, and R. Saito, *Phys. Rev. B* **94**, 075429 (2016).
 - 12 V. del Campo, J.-D. Correa, J. Correa-Puerta, D. Kroeger, and P. Haberle, *Surf. Sci.* **653**, 163 (2016).
 - 13 S. Minami, I. Sugita, R. Tomita, H. Oshima, and M. Saito, *Jap. J. Appl. Phys.* **56**, 105102 (2017).
 - 14 D. P. Adorno, L. Bellomonte and N. Pizzolato, *Eur. J. Phys.* **39**, 013001 (2017).
 - 15 M. Pizarra, C. Diaz, R. Bernardo-Gavito, J. J. Navarro, A. Black, F. Calleja, D. Granados, R. Miranda, A. L. Vazquez de Parga, and F. Martín, *J. Phys. Chem. A* **122**, 2232 (2018).
 - 16 L. M. Schoop, F. Pielnhofer, and B. V. Lotsch, *Chem. Mater.* **30**, 3155 (2018).
 - 17 J. Cano, B. Bradlyn, Zh. Wang, L. Elcoro, M. G. Vergniory, C. Felser, M. I. Aroyo, and B. A. Bernevig, *Phys. Rev. Lett.* **120**, 266401 (2018).
 - 18 S. Islam and S. S. Z. Ashraf, *Reson.* **24**, 445 (2019).
 - 19 J. Kruthoff, J. de Boer, J. van Wezel, Ch. L. Kane, and R.-J. Slager, *Phys. Rev. X* **7**, 041069 (2017).
 - 20 A. Bouhon, A. M. Black-Schaffer, and R.-J. Slager, *Phys. Rev. B* **100**, 195135 (2019).
 - 21 A. L. Araujo, R. P. Maciel, R. G. F. Dornelas, D. Varjas, and G. J. Ferreira, *Phys. Rev. B* **10**, 205111 (2019).
 - 22 E. M. Kogan and V. U. Nazarov, *Phys. Rev. B* **85**, 115418 (2012).
 - 23 E. Kogan, V. U. Nazarov, V. M. Silkin, and M. Kaveh, *Phys. Rev. B* **89**, 165430 (2014).
 - 24 E. Kogan and V. M. Silkin, *Phys. Stat. Sol. B* **254**, 1700035 (2017).
 - 25 A. H. Castro Neto, F. Guinea, N. M. R. Peres, K. S. Novoselov, and A. K. Geim, *Rev. Mod. Phys.* **81**, 109 (2009).
 - 26 C. Kittel, *Quantum Theory of Solids*, (John Wiley & Sons. Inc., New York - London, 1963).
 - 27 A. P. Sutton, *Electronic Structure of Materials*, (Clarendon Press, Oxford, 1993).
 - 28 G. G. Naumis, *Electronic properties of two-dimensional materials*, in *Synthesis, Modeling, and Characterization of 2D Materials, and Their Heterostructures*, Eds. E.-H. Yang, D. Datta, J. Ding, G. Hader (Elsevier, 2020).
 - 29 M. S. Dresselhaus, G. Dresselhaus, A. Jorio, *Group theory: Application to the physics of condensed matter*, (Springer-Verlag, Berlin - Heidelberg, 2008).
 - 30 C. Thomsen, S. Reich, J. Maultzsch, *Carbon Nanotubes: Basic Concepts and Physical Properties*, (Wiley Online Library, 2004 WILEY-VCH Verlag GmbH).
 - 31 L. D. Landau and E. M. Lifshitz, *Quantum Mechanics*, (Pergamon Press, 1991).
 - 32 D. Stewart, *Computing in Science & Engineering*, **14**, 55 (2012).
 - 33 V. M. Silkin, J. Zhao, F. Guinea, E. V. Chulkov, P. M. Echenique, and H. Petek, *Phys. Rev. B*, **80**, 121408 (2009).
 - 34 B. Borca, S. Barja, M. Garnica, D. Sánchez-Portal, V. M. Silkin, E. V. Chulkov C. F. Hermans, J. J. Hinarejos, A. L. Vázquez de Parga, A. Arnau, P. M. Echenique, and R. Miranda, *Phys. Rev. Lett.* **105**, 036804 (2010).
 - 35 S. Bose, V. M. Silkin, R. Ohmann, I. Brihuega, L. Vitali, C. H. Michaelis, P. Mallet, J. Y. Veuillen, M. A. Schneider, E. V. Chulkov, P. M. Echenique, and K. Kern, *New J. Phys.* **12**, 023028 (2010).
 - 36 T. O. Wehling, A. I. Lichtenstein, and M. I. Katsnelson, *Appl. Phys. Lett.* **93**, 202110 (2008).
 - 37 S. A. Wella, H. Sawada, N. Kawaguchi, F. Muttaqien, K. Inagaki, I. Hamada, Y. Morikawa, and Y. Hamamoto, *Phys. Rev. Mat.* **1**, 061001 (2017).
 - 38 M. Hernández, A. Cabo Montes de Oca, M. Oliva-Leyva, and G. G. Naumis, *Phys. Lett. A* **383**, 125904 (2019).
 - 39 M. Feng, J. Zhao, and H. Petek, *Science* **320**, 359 (2008).
 - 40 M. Posternak, A. Baldereschi, A. J. Freeman, E. Wimmer, and M. Weinert, *Phys. Rev. Lett.* **50**, 761 (1983).
 - 41 L. A. Agapito, M. Fornari, D. Ceresoli, A. Ferretti, S. Curtarolo, and M. B. Nardelli, *Phys. Rev. B* **93**, 125137 (2016).
 - 42 Y. B. Zhang, V. W. Brar, F. Wang, C. Girit, Y. Yayon, M. Panlasigui, A. Zettl, and M. F. Crommie, *Nat. Phys.* **4**, 627 (2008).
 - 43 T. O. Wehling, I. Grigorenko, A. I. Lichtenstein, and A. V. Balatsky, *Phys. Rev. Lett.* **101**, 216803 (2008).
 - 44 N. R. Papior, G. Calogero and M. Brandbyge, *J. Phys.: Condens. Matter* **30**, 25LT01 (2018).

- ⁴⁵ D. Niesner and T. Fauster, *J. Phys.: Condens. Matter* **26**, 393001 (2014).
- ⁴⁶ N. Armbrust, J. Güdde, and U. Höfer, *New J. Phys.* **17**, 103034 (2015).
- ⁴⁷ V. U. Nazarov, E. E. Krasovskii, and V. M. Silkin, *Phys. Rev. B* **87**, 041405(R) (2013).
- ⁴⁸ J. Jobst, J. Kautz, D. Geelen, R. M. Tromp, and S. J. van der Molen, *Nat. Commun.* **6**, 8926 (2015).
- ⁴⁹ F. Wicki, J.-N. Longchamp, T. Latychevskaia, C. Escher, and H.-W. Fink, *Phys. Rev. B* **94**, 075424 (2016).
- ⁵⁰ M. Krivenkov, D. Marchenko, J. Sanchez-Barriga, O. Rider, and A. Varykhalov, *Appl. Phys. Lett.* **111**, 161605 (2017).